

Experimental evidence for long-distance electrodynamic intermolecular forces

Mathias Lechelon, Yoann Meriguet, Matteo Gori, Sandra Ruffenach, Ilaria Nardecchia, Elena Floriani, Dominique Coquillat, Frédéric Teppe, Sébastien Mailfert, Didier Marguet, et al.

▶ **To cite this version:**

Mathias Lechelon, Yoann Meriguet, Matteo Gori, Sandra Ruffenach, Ilaria Nardecchia, et al.. Experimental evidence for long-distance electrodynamic intermolecular forces. 2021. hal-03259009v1

HAL Id: hal-03259009

https://hal.science/hal-03259009v1

Preprint submitted on 12 Jun 2021 (v1), last revised 17 Feb 2022 (v5)

HAL is a multi-disciplinary open access archive for the deposit and dissemination of scientific research documents, whether they are published or not. The documents may come from teaching and research institutions in France or abroad, or from public or private research centers.

L'archive ouverte pluridisciplinaire **HAL**, est destinée au dépôt et à la diffusion de documents scientifiques de niveau recherche, publiés ou non, émanant des établissements d'enseignement et de recherche français ou étrangers, des laboratoires publics ou privés.

Experimental evidence for long-distance electrodynamic intermolecular forces

Mathias Lechelon[1,2,3], Yoann Meriguet[4,5], Matteo Gori[1,2,6], Sandra Ruffenach[5], Ilaria Nardecchia[1,2,3], Elena Floriani[1,2], Anastasiia Kudashova[4,5], Dominique Coquillat[5], Frédéric Teppe[5], Sébastien Mailfert[3], Didier Marguet[3], Pierre Ferrier[3], Luca Varani[4], James Sturgis[7], Jeremie Torres[4], Marco Pettini[1,2]

[1]Aix Marseille Univ, Université de Toulon, CNRS, CPT, Marseille, France

[2]CNRS Centre de Physique Théorique UMR7332, 13288 Marseille, France

[3]Centre d'Immunologie de Marseille-Luminy, 13288 Marseille, France

[4]Institut d'Electronique et des Systèmes (IES), University of Montpellier - CNRS, Montpellier, France

[5]Laboratoire Charles Coulomb (L2C), University of Montpellier - CNRS, Montpellier, France

[6]Quantum Biology Lab, Howard University, 2400 6th St NW, Washington, DC 20059, USA

[7]Laboratoire d'Ingenierie des Systèmes Macromoleculaires UMR7255, 13402 Marseille, France

E-mail: jeremie.torres@umontpellier.fr; corresponding author

E-mail: marco.pettini@cpt.univ-mrs.fr; corresponding author

June 12, 2021

Abstract

Both Classical and Quantum Electrodynamics predict the existence of dipole-dipole long-range electrodynamic intermolecular forces, however these have never been hitherto experimentally observed. The discovery of completely new and unanticipated forces acting between biomolecules could have considerable impact on our understanding of the dynamics and functioning of the molecular machines at work in living organisms. Here, using two independent approaches, we demonstrate experimentally for the first time the activation of resonant electrodynamic intermolecular forces. We characterize clustering transitions induced by these forces by fluorescence correlation spectroscopy when out-of-equilibrium conditions induce collective molecular oscillation observed by Terahertz (THz) spectroscopy. This is an unprecedented experimental *proof of principle* of a physical phenomenon that, having been observed for bio-macromolecules and with a long-range of action (up to 1000 $\mathring{A}$), could be of importance for biology. Therefore, in addition to thermal fluctuations that drive molecular motion randomly, these resonant (and thus selective) electrodynamic forces may contribute to molecular encounters in the crowded cellular space. We anticipate our findings will provide a basis for future systematic deepening of physical aspects of the reported phenomena and for future systematic assessment of the relevance of electrodynamic forces in shaping the dynamics of biomolecular encounters and recognition in biology.

Main

Beyond the strong interest for fundamental physics of observing intermolecular dipole-dipole electrodynamic (ED) forces, this experimental study to detect these forces was highly motivated by their possible role at the molecular level in biology. Indeed, from a physicists point of view, living matter offers a wealth of fascinating dynamic phenomena involving biomolecules (proteins and nucleic acids) organized in an intricate and complex network of biochemical interactions providing astonishing efficiency. In numbers, a single cell presents at any given time about 130,000 binary interactions between proteins [1, 2]. The forces hitherto considered in biological contexts are of (quasi-) electrostatic nature (chemical-, and hydrogen-bonds, bare Coulomb, Van-der-Waals London, Hamaker-forces) and are limited to a range of action shorter than 10 $\mathring{A}$ due to Debye screening by small freely moving ions in the intracellular water. Such interactions are relevant for stereo-specific, "key-lock" and "induced-fit" interactions at short distances but hardly effective to recruit distant molecules. Thus, understanding how the right molecule gets to the right place, at the right moment, in the right cascade of events of any

biological action is one of the most striking challenges. Fundamentally, it is assumed that this network of interactions is dominated by random molecular diffusion throughout the cellular spaces in which, sooner or later, a molecule will encounter its cognate partners. However, free diffusion is considerably slowed down in a highly crowded environment [3] as in the case of the cell interior. Moreover, when diffusion measurements are performed in complex molecular organizations such as those of living cells, most of the biomolecules show anomalous rather than Brownian diffusion [4, 5]. Furthermore, structuring of the cytosol into phase-separated domains [6, 7], substrate channeling of the metabolons [8], or long-distance interactions in DNA searching [9] and organization [10] have recently come to the forefront to question the discrepancy between the observed reaction rates in cells with the predictions of a strict random diffusion model [6, 11]. Within this framework, dipole-dipole electrodynamic interactions are predicted to promote molecular attraction by being selective through resonance and to act over long distances [12]. These forces can propagate without attenuation in electrolytes of ionic strength comparable to that in the cytoplasm, provided that their oscillation frequency exceeds few hundreds of MHz [13], since at such frequencies the Debye screening is ineffective [14]. Therefore, we hypothesize that, in addition to random diffusion, selective long-range attractive electrodynamic interactions increase the encounter rates between A and B cognate partners through a mutual force field described by a potential $U(r)$ where r is the intermolecular distance. Then, after the Smoluchowski-Debye formula [15, 16], the association rate is given by $k_a^* = 4\pi R^*(D_A + D_B)$ where $D_{A,B}$ are their diffusion coefficients and R^* is given by

$$R^* = \left[\int_{R_A+R_B}^{\infty} \frac{e^{U(r)/kT}}{r^2} dr \right]^{-1}. \tag{1}$$

where R_A, R_B are the hydrodynamic radii of A and B, respectively; k is the Boltzmann constant and T the temperature. Remarkably, for an attractive interaction, $U(r) < 0$, Equation (1) implies $k_a^* > k_a = 4\pi(R_A + R_B)(D_A + D_B)$, that is, an increase of the association rate with respect to the purely diffusive k_a. However, electrodynamic macromolecular interactions have not previously been considered for several reasons, including: *i)* they have never been observed in any experimental context, though theoretically predicted by both Classical [12, 17] and Quantum Electrodynamics [18]; *ii)* they require an out-of-equilibrium system, which though, of course, found in all living systems, is hard to organize in the laboratory *in vitro*, especially with molecules in metastable states with strongly excited giant dipole vibrations, as required for such interactions; *iii)* out-of-equilibrium collective vibrations of macromolecules are expected

in the $0.1-1.0$ THz domain, this is experimentally challenging to observe because of the strong absorption of water, and indeed such vibrations have only recently been detected for the first time [19]. Interestingly, the coherence of these collective molecular vibrations is theoretically expected to be long-lived [20].

Here we demonstrate experimentally the activation of long-range attractive electrodynamic forces between proteins. This was made possible through the study of R-Phycoerythrin (R-PE), a protein that can be excited naturally by an external energy supply, a light source. Then, by working at different concentrations (i.e. intermolecular distances) and excitation power of a laser as the light source, we have achieved what follows: *i)* observation of the activation of collective intramolecular oscillation of the proteins, a necessary pre-requisite to activate the physical mechanism pictorially outlined in Figure 1a; *ii)* observation of a distributed-clustering transition dependent on activation of these collective molecular oscillations, as expected after a thorough preparatory work [3, 21, 22, 23], and *iii)* the consequent expected change of the frequency of the collective oscillation [24]. For this, two experimental techniques were used, THz spectroscopy and fluorescence fluctuation spectroscopy (Figure 1b,c). Overall, our experimental work supports a *proof-of-principle* that out-of-equilibrium collective oscillations are capable of activating dipole-dipole electrodynamic intermolecular forces, thus paving the way to explore the potential role of ED intermolecular forces in living matter.

Results

This first experimental study has been performed with a natural light-harvesting protein derived from red algae, the R-PE (Extended Data Figure 6). This protein naturally contains a total of 38 fluorochromes, phycoerythrobilin and phycourobilin (the terminal acceptor of energy).

These pigments are highly sensitive to the $\lambda = 488$ nm light used in these experiments. By illuminating the R-PE molecules in saline solution each molecule can enter a coherent vibrational state (Figure 2) displaying similar phenomena to those reported for Bovine Serum Albumin (BSA) protein in [19]: the existence of a threshold for the energy input rate to activate the collective mode, and a saturation of the oscillation amplitude at high values of the energy input rate. Two collective oscillation frequencies for R-PE are found. One at 0.071 THz ($=$ 2.4 cm^{-1}) and another at 0.096 THz ($=$ 3.2 cm^{-1}) (see Extended Data Figure **??**). Let us schematize the R-PE protein as a doughnut-shaped object of $M = 240$ kDalton, with a larger midline radius $R = 37.5$ $\mathring{A}$, a minor radius $r = 30$ $\mathring{A}$ [25], density ρ (the ratio between M and the volume of the torus), and Young elastic modulus E. The frequencies of the collective

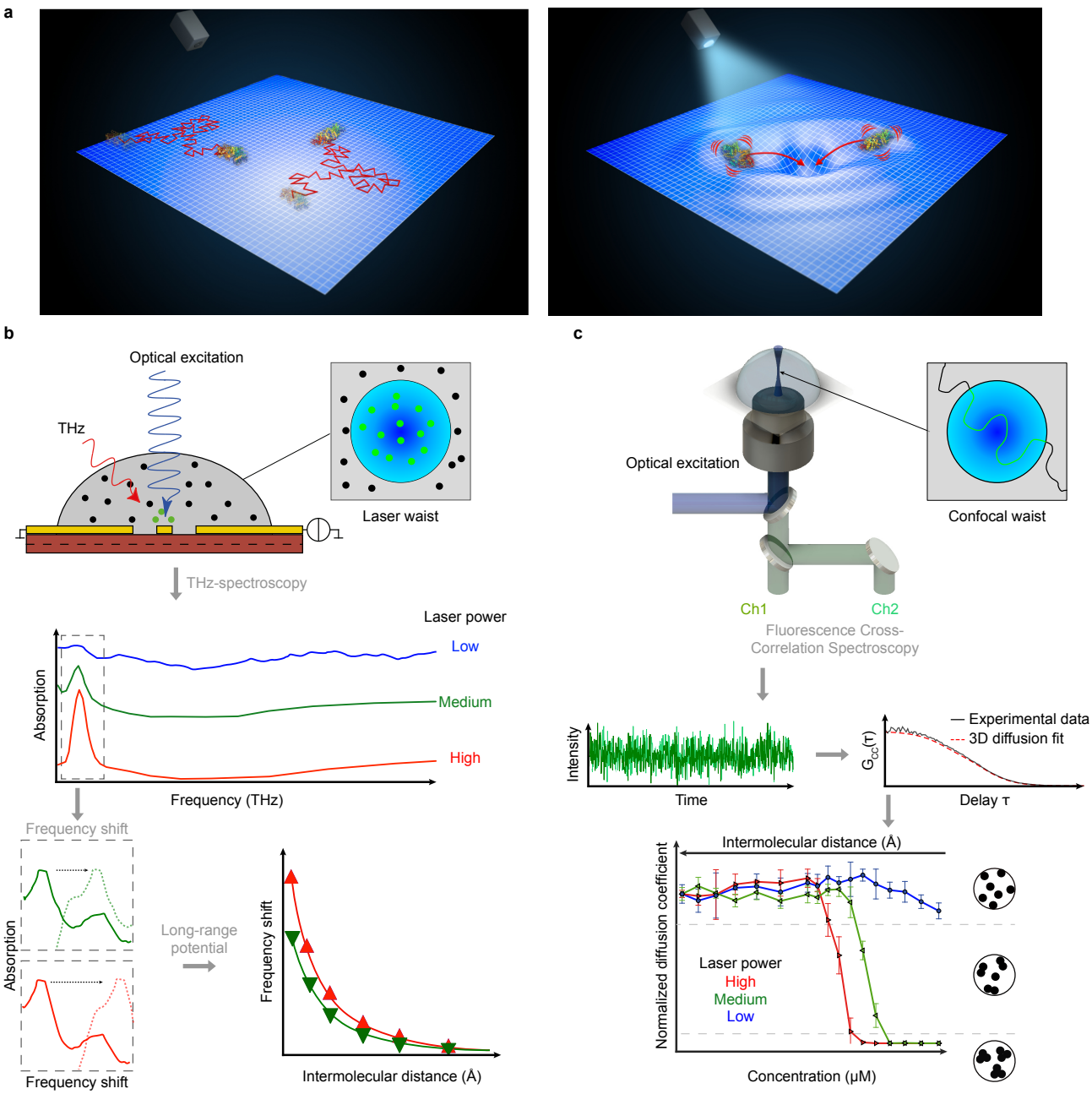


Figure 1: Long-range electrodynamic interactions - Principle and experimental approaches (a) At thermal equilibrium, macromolecules show a Brownian diffusive motion in solution (left panel). By switching-on an external energy source, molecules are in an out-of-thermal equilibrium collective vibrational state that can generate ED forces through associated large dipolar resonant oscillations (right panel). (b) In THz spectroscopy, the frequency of the collective vibration varies as a function of the average intermolecular distance (determined by the protein concentration). With respect to the reference frequency at "infinite" dilution, a frequency-shift inversely proportional to the cubic power of the average intermolecular distance is theoretically expected if the proteins interact through ED forces. (c) In FCS, the transit times of the proteins across the volume of observation are measured, hence the protein diffusion coefficients. Under out-of-thermal equilibrium conditions, the theory predicts a phase transition due to ED forces clustering proteins. This should be observed at a given protein concentration by a sudden drop in the diffusion coefficient from its Brownian value. In both (b) and (c), out-of-thermal equilibrium is activated by optical excitation.

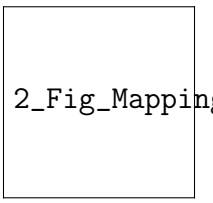


Figure 2: Collective oscillation of the R-PE measured by THz-Spectroscopy. Absorption strength of the R-PE (1 mg/mL in 200 mM NaCl) as a function of detection frequency and the laser power activating the molecular collective oscillation at a frequency of 71 GHz (2.4 cm^{-1}). The absorption line profile (bottom) indicated by the horizontal white dashed line was measured at an optical power of 31.5 mW, while the laser power threshold (left) behaviour is indicated by the black dashed line. Stars stand for experimental data.

extension modes (those corresponding to oscillating larger radius R) are given by [26]

$$\nu_n = \frac{(1+n^2)^{1/2}}{2\pi R}\left(\frac{E}{\rho}\right)^{1/2}, \tag{2}$$

whence the ratio $\nu_1/\nu_0 = \sqrt{2} \simeq 1.41$ which approximates within a 4% the ratio between the observed frequencies, that is $0.096/0.071 = 1.35$. The Young modulus of R-PE is not known in the literature, but by inverting the above formula we obtain $E \simeq 5.3$ GPa which seems reasonable knowing that at 300 K for Myoglobin $E \simeq 3.5$ GPa, and for BSA $E \simeq 6.75$ GPa [27] (both proteins being mostly made of α-helices like R-PE).

A theoretically expected signature of attractive electrodynamic forces among macromolecules vibrating at the same frequency is a phase transition between a dispersed phase of rapidly diffusing molecules, and a clustered phase of very slowly moving aggregates of molecules [22] (see [28]). The control parameter of this transition is the average intermolecular distance, which is set by adjusting the molecular concentration.

In the fluorescence correlation spectroscopy (FCS) experiments, the protein concentrations $\mathcal{C}$ have been varied in the interval between 0.1 μM and 10 μM to make the average intermolecular distance $\langle r \rangle = \mathcal{C}^{-1/3}$ vary in the interval $550 - 1950$ $\mathring{A}$.

The ionic strength of the protein solution is kept at 200 mM by means of suitable concentrations of NaCl in water. This ensures a good shielding of electrostatic interactions. Moreover, the laser power ($\lambda = 488$ nm) has been varied between 50 and 150 μW. In Extended Data Figures 9 and 10, typical fluorescence traces are reported for different laser powers and protein concentrations.

The diffusion times τ_D determined from the Cross Correlation Functions (CCFs) of fluorescence traces, and the measured waist of the confocal volume where the molecules are both excited and observed, allow estimation of the diffusion coefficients D. The use of CCFs is mo-

tivated in section Methods and in Extended Data Figures 7 and 8. The values of the diffusion coefficient D are normalized with respect to the Brownian values D_0 of each data series recorded at a given laser power (Figure 3). At low laser power the measured value of D_0 matches the expected theoretical one $D_0 = k_B T/(6\pi\eta R_H)$, with η the viscosity of the solution, and R_H the hydrodynamic radius of the protein. At laser power of 50 μW, the observed values of D (blue circles) do not change with the intermolecular distance. The diffusion of the R-PE molecules is Brownian for all the concentrations considered. This means that the energy input rate is either below the threshold value required to excite molecular collective vibrations, or the intermolecular ED forces are very weak because of the small amplitude of the collective vibrations of the R-PE proteins. The mismatch between the laser power values mentioned in Figure 2 for THz experiments and those reported above for diffusion experiments is due to the different volumes illuminated (see Methods).

At higher laser power, 100 μW, obviously and consistently with a thermal effect, the measured value of D_0 at low concentration is larger than in the preceding case. However it cannot explain, in the interval of inter-molecular distances $700 - 750$ $\mathring{A}$ (green triangles), the steep drop of D/D_0 that correlates with the increase of the fluorescence fluctuations and a sudden increase of the diffusion time τ_D.

At the highest laser power considered, 150 μW, again the steep drop of D/D_0 is observed but now in the interval of inter-molecular distances $900 - 950$ $\mathring{A}$ (red triangles). In both cases, the steep drop of D/D_0 correlates with a strong increase of the fluorescence fluctuations and a sudden and huge increase by several orders of magnitude of the diffusion time τ_D.

The steep drop of D/D_0 and the increased amplitude of fluorescence fluctuations are the observable effects of a clustering phase transition stemming from the competition between the electrodynamic intermolecular attractive forces and thermal fluctuations. This is confirmed theoretically by a semi-analytical model, by Molecular Dynamics simulations and by Monte Carlo computations (see Methods and [28]). In Figure 3b two snapshots are shown of numerical Monte Carlo computations performed by considering long-range electrodynamic interparticle forces. Thus, the appearance of clusters predicted theoretically has been experimentally observed through the sudden enhancement of fluorescence fluctuation amplitudes and long transit times across the confocal volume of the FCS setup. Clusters of R-PE were visually evidenced by fluorescence microscopy (Extended Data Fig.14 and Video online).

Increasing the laser power, the higher the power the stronger the collective oscillation of R-PE molecules and the larger the associated oscillating dipole moment. Hence the displacement of the clustering transition to a greater average intermolecular distance for the stronger

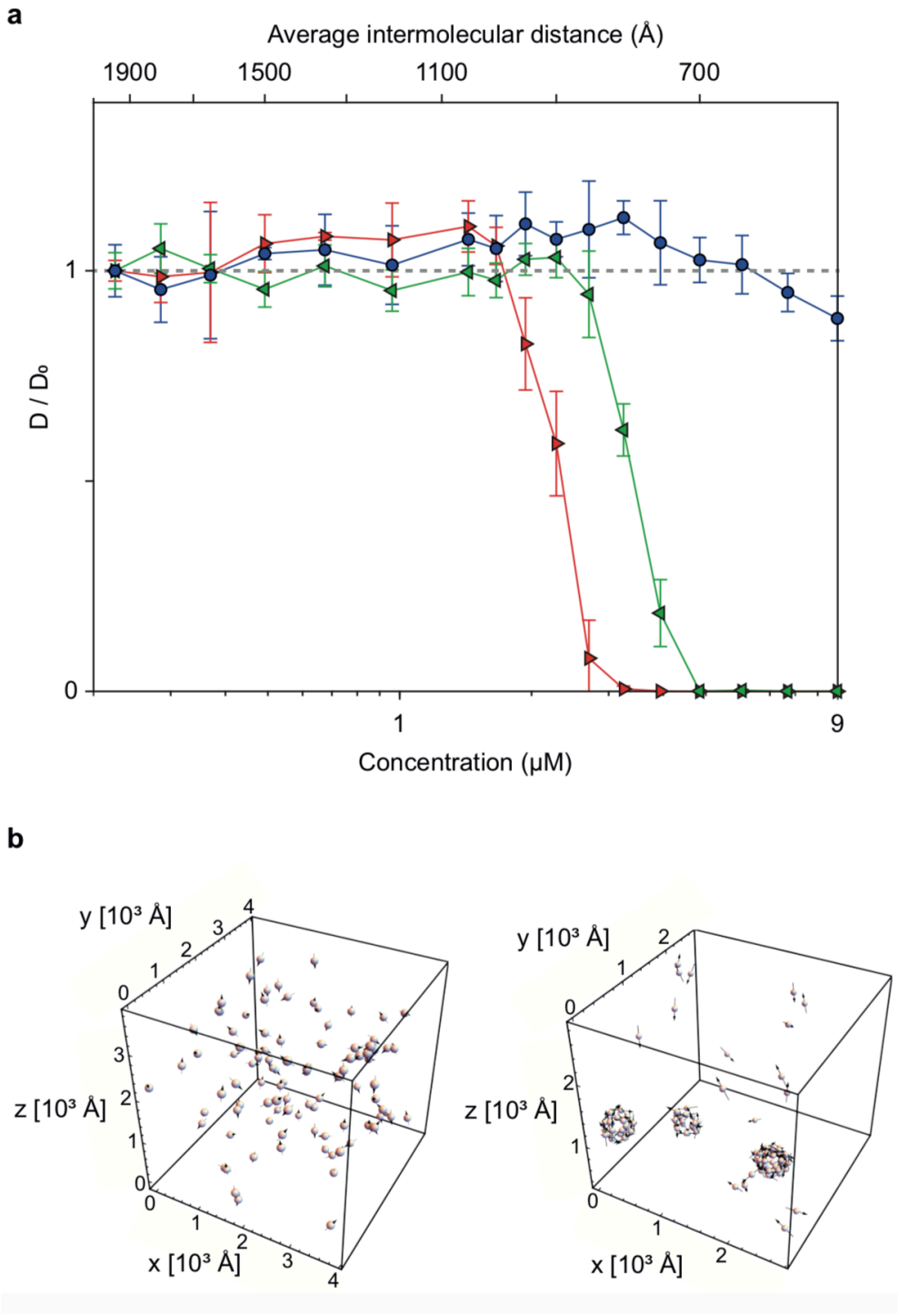


Figure 3: Effect of protein concentration and laser power illumination on R-PE diffusion: Clustering phase transition. (a) Diffusion coefficients normalized to the Brownian D_0 values measured for each data series at 0.223 μM ($\langle r \rangle \simeq 1950$ $\mathring{A}$) and recorded at 50 μW (blue circles), 100 μW (green triangles), and 150 μW (red triangles). Each point corresponds to the average of 5 independent experiments. (b) Snapshots of numerical Monte Carlo computations involving long-range electrodynamic inter-particle forces obtained with different initial values of $\langle r \rangle$. With $\langle r \rangle_{initial} \simeq 1000$ $\mathring{A}$ the system remains in the dispersed phase (lower left box) where $D/D_0 = 1$ (Brownian diffusion); with $\langle r \rangle_{initial} \simeq 950$ $\mathring{A}$ the system switches to the clustered phase with D/D_0 very small (lower right box).

molecular oscillations. Consistently, by suddenly lowering the power of the laser light supply in the clustered phase a rapid disaggregation of the clusters is observed, as shown in Figures 13 of Extended Data.

All these results are a clearcut proof of the activation of electrodynamic intermolecular attractive forces due to the collective vibrations of the R-PE molecules.

An independent confirmation of the activation of electrodynamic intermolecular attractive forces is obtained by measuring the shift of the collective vibrational frequency as a function of the concentration of molecules. Once again the proteins were observed in aqueous solution with the addition of 200 mM of NaCl to screen electrostatic interactions. In fact, theory predicts that electrodynamic dipole-dipole interaction between two molecules results in a shift $\Delta\nu$ of their vibration frequency from the unperturbed frequency ν_0, shift proportional to $1/r^3$ with r the intermolecular distance [12]. Remarkably, this law is preserved also for a large number of interacting molecules, that is, the frequency shift is proportional to $1/\langle r\rangle^3$ where $\langle r\rangle$ is the average intermolecular distance given by $\langle r\rangle = \mathcal{C}^{-1/3}$ (see [28] for the theoretical explanation). The unperturbed vibration frequency ν_0 is operationally measured at very low molecular concentration. The shifts $\Delta\nu$ are then measured with respect to this value of ν_0.

The collective oscillation frequency of the R-PE at 0.071 THz (i.e. 2.4 cm^{-1}) allowed to use as THz detector an electronic nano-device, namely a bow-tie antenna on the 2D electron gas layer of a FET transistor called a rectenna [29, 30, 31, 32, 33] (see Methods Figure 5a). The measured frequency shift is found to follow a linear dependence on the protein concentration, that is, the experimental outcomes are in excellent agreement with the theoretical predictions (Figure 4a). The steepening of the fitted lines in Figure 4a as laser power is increased is also in agreement with expectations. This is because the increasing oscillation amplitude (entailing a larger oscillating dipole moment), results in stronger intermolecular electrodynamic interaction and hence a larger frequency shift (for theoretical details see [28]). The case of R-PE is especially important because two independent experimental approaches lead to the same physical conclusion: the activation of intermolecular electrodynamic forces acting at a long distance. Thus the possibility of artefacts or misinterpretations is ruled out. Importantly, these forces are not peculiar of the R-PE since they are also observed by making measurements with another protein, BSA. BSA molecules were labeled with an average number of 5 fluorochromes AF488 5-TFP, covalently bonded to the Lysine residues, excitable by the light emitted by a diode laser at 488 nm. The reason for considering the BSA is twofold: first, the labeled BSA molecules, when continuously supplied by laser light at $\lambda = 488$ nm, are driven in a collective vibration

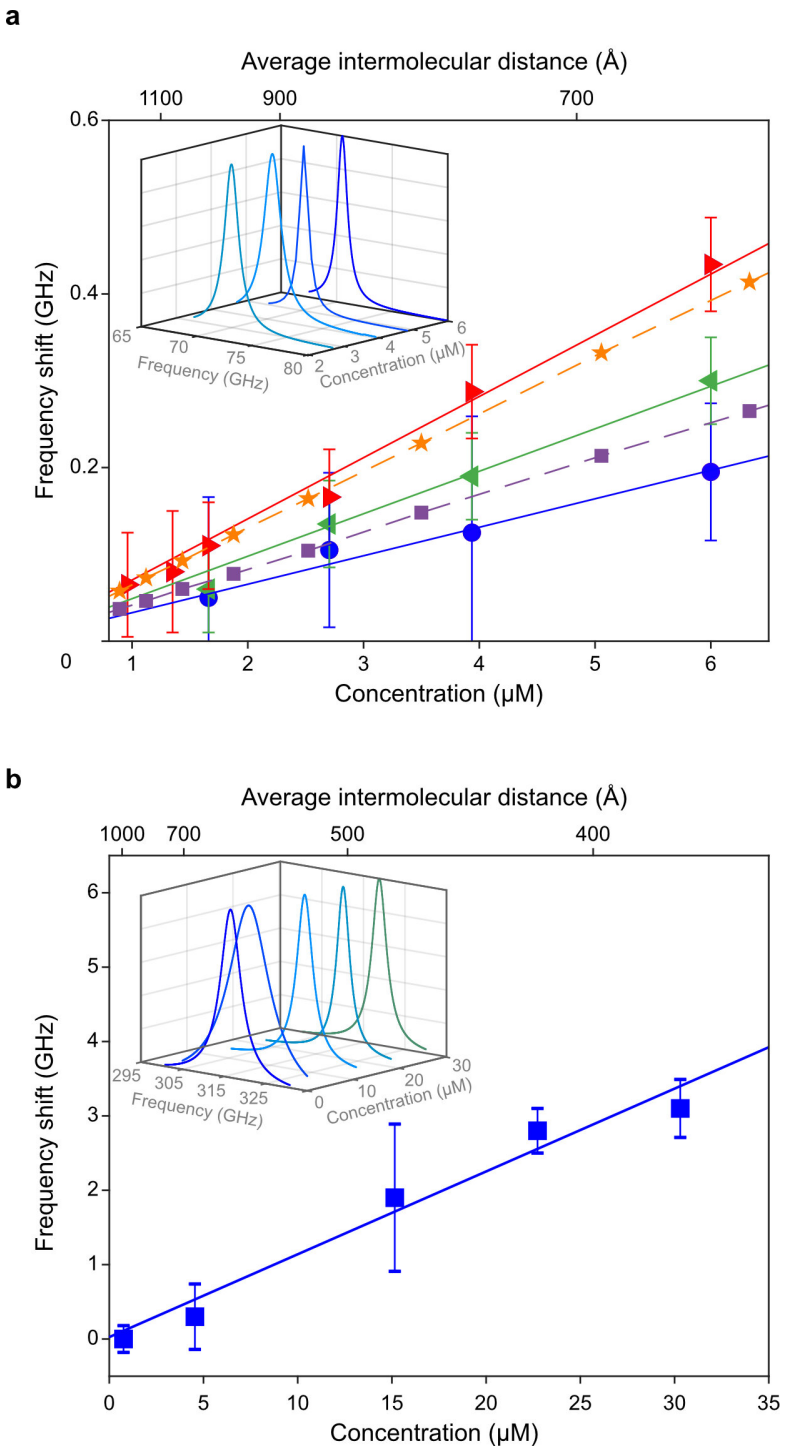


Figure 4: Frequency shifts of the intramolecular collective vibrations of R-PE and BSA at different concentrations. (a) Measurements for R-PE were performed at 30^o C in 200 mM of NaCl. The shift is relative to the reference frequency measured at the lowest protein concentration. Measurements have been performed at different powers of the laser: 31.5 mW (blue circles), 39.5 mW (green triangles), 50 mW (red triangles). Purple squares and orange stars refer to theoretical outcomes worked out with different values of molecular dipole moments (see [28]). (b) Measurements for BSA were performed at 30^o C in 200 mM of NaCl at a laser power of 40 mW. Insets: Lorentz fits of the resonances as a function of concentration and for maximal optical power.

mode at 0.314 THz (i.e. 10 cm^{-1}) [19]; second, R-PE and BSA both have a structure composed largely of alpha-helices (Extended Figure 1), a property supposed to facilitate the activation of collective vibrational modes.

The collective oscillation frequency of the BSA at 0.314 THz required the use of a near-field microwire-based probe coupled with a wave-guide (see Methods Figure 5b). Again, the measured frequency shift is found to follow a linear dependence on the protein concentration as expected (Figure 4b). This provides a remarkable confirmation of the activation of long distance electrodynamic interactions also for BSA.

It is worth pointing out that the two THz experimental setups have been operated at a different spatial density of the laser light, with respect to diffusion experiments, to prevent a clustering transition during the frequency shift measurements (see Methods).

Discussion

In the work presented here, we have experimentally shown, for the first time, that the excitation of out-of-equilibrium collective oscillations is capable of driving molecular association through the activation of electrodynamic intermolecular forces. R-PE provides convincing evidence for these forces using a pair of complementary experimental approaches. Thus, R-PE represents the *"Rosetta stone"* allowing us to identify attractive intermolecular forces through two completely different physical effects.

Long-range electrodynamic interactions have also been activated using a second protein, fluorescent dye-labeled BSA. These results confirm the generality of this phenomenon thus paving the way for the experimental searching of ED forces in the more complex environment encountered in cell biology.

A central feature of the ED forces activated by collective molecular vibrations is their long-range property, that is, they stem from an interaction potential decreasing as the third inverse power of the intermolecular distance. This generates first-order phase transitions with the formation of molecular condensates. A thorough theoretical analysis of this transitional behavior, and of the frequency shift of the collective vibrations of the proteins, caused by their interaction through ED forces, can be found in [28].

By being dynamic and reversible, ED forces can be instrumental in structuring the mesoscale molecular organization through the formation of biomolecular condensates and thus provide a rationale to explain the speed of many cellular processes. While we have evidence of the association of biological macromolecules driven by ED forces *in vitro*, the conditions are far

from the ones found *in cellulo*. Here, the energy sources necessary to maintain the molecules out-of-equilibrium need to be characterized. Among the potential candidates, there are: adenosine triphosphate (ATP) as a universal biological fuel, ionic currents such as those used to drive ATP synthesis, ionic collisions, photons produced by mitochondria, or external light. The notion of selectivity of ED forces will also need to be explored in a crowded environment composed of a vast diversity of molecular components. More specifically, it will be important to consider the possible role of ED forces between different molecular species (ligand-receptor, DNA-protein) co-resonating at one or more collective oscillation frequencies.

Moreover, our findings could be of general interest for methodological applications requiring a tight control in space and time of molecular interactions in living cells to decipher cellular functions. As an example, in the developing field of optogenetics where molecular interactions are switched on/off by engineered proteins controlled by light [34].

Further, ED forces could also be exploited in the domain of drug design. It has been hypothesized that combining steric complementarity with "long-range complementarity" could improve therapeutic efficiency. Thus, ED forces could allow recognition at a distance and drive an efficient mutual approach between a drug and its therapeutic target before their final chemical binding [35].

Finally, throughout evolution, life has exploited all the available physical laws, processes, and phenomena. It is thus exciting to speculate how the new phenomenon reported here for the first time has been used to gain adaptive advantage and possibly overcome some of the adverse effects of molecular crowding in cells.

References

[1] Bonetta, L. Interactome under construction. *Nature* **468**, 851–852 (2010).

[2] Venkatesan, K. & et al. An empirical framework for binary interactome mapping. *Nature Methods* **6**, 83 – 90 (2009).

[3] Gori, M., Donato, I., Floriani, E., Nardecchia, I. & Pettini, M. Random walk of passive tracers among randomly moving obstacles. *Theoretical Biology and Medical Modelling* **13**, 13–33 (2016).

[4] Banks, D. S. & Fradin, C. Anomalous diffusion of proteins due to molecular crowding. *Biophysical Journal* **89**, 2960 – 2971 (2005).

[5] Golan, Y. & Sherman, E. Resolving mixed mechanisms of protein subdiffusion at the t cell plasma membrane. *Nature Commun* **8**, 15851–15866 (2017).

[6] Banani, S., Lee, H., Hyman, A. & Rosen, M. Biomolecular condensates: organizers of cellular biochemistry. *Nature Rev. Mol. Cell Biol.* **18**, 285 – 298 (2017).

[7] Berry, J., Brangwynne, C. P. & Haataja, M. Physical principles of intracellular organization via active and passive phase transitions. *Reports on Progress in Physics* **81**, 046601 (2018).

[8] Sweetlove, L. J. & Fernie, A. R. The role of dynamic enzyme assemblies and substrate channelling in metabolic regulation. *Nature Communications* **9**, 2136 (2018).

[9] Kulaeva, O. I., Nizovtseva, E. V., Polikanov, Y. S., Ulianov, S. V. & Studitsky, V. M. Distant activation of transcription: Mechanisms of enhancer action. *Molecular and Cellular Biology* **32**, 4892 – 4897 (2012).

[10] Wang, J. *et al.* Exploring the mechanisms of genome-wide long-range interactions: interpreting chromosome organization. *Briefings in Functional Genomics* **15**, 385–395 (2016).

[11] Wheeldon, I., Minteer, S., Banta, S. & et al. Substrate channelling as an approach to cascade reactions. *Nature Chemistry* **8**, 299 – 309 (2016).

[12] Preto, J., Pettini, M. & Tuszynski, J. A. Possible role of electrodynamic interactions in long-distance biomolecular recognition. *Phys. Rev. E* **91**, 052710–052728 (2015).

[13] de Xammar Oro, J. R., Ruderman, G. & Grigera, J. R. Electrodynamics of interactions in electrolyte media. possible consequences in biological functions. *Biophysics* **53**, 195 (2008).

[14] Maxwell, J. C. *A Treatise on Electricity & Magnetism* (Dover Publications Inc., New-York, 1954).

[15] Debye, P. Reaction rates in ionic solutions. *Transactions of The Electrochemical Society* **82**, 265 (1942).

[16] Noyes, R. M. Effects of diffusion rates on chemical kinetics. *Prog. React. Kinet.* **1**, 129 (1961).

[17] Fröhlich, H. Long-range coherence in biological systems. *Rivista Nuovo Cimento* **7**, 399 – 418 (1977).

[18] Salam, A. *Molecular Quantum Electrodynamics* (John Wiley and Sons, Inc., New Jersey, 2010).

[19] Nardecchia, I., Torres, J., Sturgis, J., Pettini, M. & et al. Out-of-equilibrium collective oscillation as phonon condensation in a model protein. *Phys. Rev. X* **8**, 031061 (2018).

[20] Zhang, Z., Agarwal, G. S. & Scully, M. O. Quantum fluctuations in the fröhlich condensate of molecular vibrations driven far from equilibrium. *Physical Review Letters* **122**, 158101–158107 (2019).

[21] Preto, J., Floriani, E., Nardecchia, I., Ferrier, P. & Pettini, M. Experimental assessment of the contribution of electrodynamic interactions to long-distance recruitment of biomolecular partners: Theoretical basis. *Phys. Rev. E* **85**, 041904 (2012).

[22] Nardecchia, I., Gori, M., Floriani, E., Pettini, M. & et al. Experimental detection of long-distance interactions between biomolecules through their diffusion behavior: Numerical study. *Phys. Rev. E* **90**, 022703 (2014).

[23] Nardecchia, I., Lechelon, M., Gori, M., Pettini, M. & et al. Detection of long-range electrostatic interactions between charged molecules by means of fluorescence correlation spectroscopy. *Phys. Rev. E* **96**, 022403 (2017).

[24] Olmi, S., Gori, M., Donato, I. & Pettini, M. Collective behavior of oscillating electric dipoles. *Scientific Reports* **8**, 15748 (2018).

[25] Chan, W.-r. & et al. Crystal structure of r-phycoerythrin from polysiphonia urceolata at 2.8 $\AA$ resolution. *Journal Molecular Biology* **262**, 721 – 731 (1996).

[26] Blevins, R. D. *Formulas for natural frequency and mode shape* (Van Nostrand Reinhold Company, New-York, 1979).

[27] Perticaroli, S. *et al.* Secondary structure and rigidity in model proteins. *Soft Matter* **9**, 9548–9556 (2013).

[28] Gori, M., Floriani, E. & Pettini, M. Theoretical proposals for the experimental detection of electrodynamic interactions between biomolecules. *https://hal.archives-ouvertes.fr/hal-03257350* (2021).

[29] Dyakonov, M. & Shur, M. Shallow water analogy for a ballistic field effect transistor: New mechanism of plasma wave generation by dc current. *Phys. Rev. Lett.* **71**, 2465–2468 (1993).

[30] Knap, W. *et al.* Nonresonant detection of terahertz radiation in field effect transistors. *Journal of Applied Physics* **91**, 9346–9353 (2002).

[31] Nouvel, P. *et al.* Terahertz spectroscopy of plasma waves in high electron mobility transistors. *Journal of Applied Physics* **106**, 013717–013729 (2009).

[32] Dyakonov, M. I. Generation and detection of terahertz radiation by field effect transistors. *Comptes Rendus Physique* **11**, 413 – 420 (2010).

[33] Schuster, F. *et al.* Broadband terahertz imaging with highly sensitive silicon cmos detectors. *Opt. Express* **19**, 7827 – 7832 (2011).

[34] Tischer, D. & Weiner, O. D. Illuminating cell signalling with optogenetic tools. *Nature Rev. Mol. Cell Bio.* **15**, 551 – 558 (2014).

[35] Veljkovic, N., Glisic, S., Perovic, V. & Veljkovic, V. The role of long-range intermolecular interactions in discovery of new drugs. *Expert Opinion Drug Discovery* **6**, 1263–1270 (2011).

[36] Painter, P., Mosher, L. & Rhoads, C. Low-frequency modes in the raman spectra of proteins. *Biopolymers* **21**, 1469–1472 (1982).

[37] Painter, P. C., Mosher, L. & Rhoads, C. Low-frequency modes in the raman spectrum of dna. *Biopolymers* **20**, 243–247 (1981).

[38] Fröhlich, H. Long-range coherence and energy storage in biological systems. *International Journal of Quantum Chemistry* **2**, 641– 649 (1968).

[39] Fröhlich, H. Long range coherence and the action of enzymes. *Nature* **228**, 1093 (1970).

[40] Fröhlich, H. Selective long range dispersion forces between large systems. *Physics Letters A* **39**, 153–154 (1972).

[41] Haustein, E. & Schwille, P. Fluorescence correlation spectroscopy: Novel variations of an established technique. *Annual Review of Biophysics and Biomolecular Structure* **36**, 151–169 (2007). PMID: 17477838.

[42] Petrášek, Z. & Schwille, P. Precise measurement of diffusion coefficients using scanning fluorescence correlation spectroscopy. *Biophysical Journal* **94** (2008).

[43] Laurence, T. & et al. Fluorescence correlation spectroscopy at micro-molar concentrations without optical nanoconfinement. *Journal of Physical Chemistry* **B118**, 9662 – 9667 (2014).

[44] Khatua, S. & et al. Enhanced-fluorescence correlation spectroscopy at micro-molar dye concentrations around a single gold nanorod. *Physical Chemistry Chemical Physics* **17**, 21127 – 21132 (2015).

[45] Zhao, M. *et al.* Afterpulsing and its correction in fluorescence correlation spectroscopy experiments. *Applied Optics* **42**, 4031 – 4036 (2003).

[46] Magde, D., Elson, E., Hyman, A. & Webb, W. Fluorescence correlation spectroscopy. ii. an experimental realization. *Biopolymers* **13**, 29 – 61 (1974).

[47] Keilmann, F. Fir microscopy. *Infrared Phys. Techno.* **36**, 217–224 (1995).

METHODS

Theoretical rationale

A crucial condition to activate long-range electrodynamic forces between biomolecules is to put them out-of-thermal-equilibrium, in a coherent vibrational state of all - or a large fraction - of their atoms. In fact, at thermal equilibrium a macromolecule "flickers", that is, it undergoes incoherent and random deformations of all its subunits resulting in small noisy variations of its static dipole moment. At equilibrium, energy equipartition among the normal modes of vibration holds, thus the amplitude of collective modes is very small. Collective modes have been detected at equilibrium already a long time ago for proteins [36] and polynucleotides [37] with Raman and far infrared spectroscopy. But by keeping a macromolecule out of thermal equilibrium by means of an external energy supply a phonon condensation phenomenon can be activated [19], consisting of the channelling of the supplied energy into a low frequency coherent mode of vibration of all the atoms (or of a significant fraction of them) of the same macromolecule. So excited, the macromolecule may have a very large oscillating dipole moment. In turn, in such a collective oscillation state, a biomolecule could activate a long-range attractive electrodynamic interaction with other molecules if they possess a proper frequency close to that of the coherent mode. This scenario has been proposed a long time ago [38, 39, 40, 17] but has been marginalized for several reasons, including its quantum mechanical formulation and because it has never been given experimental evidence. Reformulated in a classical framework [12, 19], the above sketched scenario has been given new credit after the recent experimental proof of the possibility of activating a stationary oscillation of a macromolecule out of thermal equilibrium [19]. This is a necessary pre-condition to activate long-range electrodynamic interactions [12]. It is worth mentioning that in a recent work it has been convincingly maintained that a full understanding of Fröhlich condensation can come solely from a quantum theory [20].

Theoretical design of the experiments

A first method designed to detect long-range electrodynamic intermolecular forces is based on the expected change in the diffusion properties of the proteins at different concentrations, in the presence of both suitably activated electrodynamic forces and stochastic forces representing the random hits of water molecules on the proteins. The feasibility study of this approach has been carried out via theoretical computations resorting to Molecular Dynamics simulations. Experimentally, the FCS/FCCS methods that are based on recording the fluctuations of fluorescence

signal in a small volume of observation (i.e., a confocal volume in FCS microscopy) have the sensitivity to infer information about the diffusion time through this volume [41]. The autocorrelation (cross-correlation) function of the detected fluorescence signal is fitted by means of an analytic formula derived by a theoretical model of diffusion. Hence the diffusion time τ_D, that corresponds to the average time molecules stay within the volume of observation, is obtained and the diffusion coefficient D is simply given by $D = \omega_{xy}^2/4\tau_D$, where ω_{xy}^2 is the lateral waist of the excitation beam focused through the objective of the microscope. This allows us to assess whether the transit time of fluorescent molecules follows a Brownian diffusion law (i.e., resulting from stochastic forces generated by collisions with water molecules) or, instead, a law that possibly combines both electrodynamic forces and the stochastic forces just mentioned. A three steps feasibility study has validated this experimental strategy to detect these electrodynamic intermolecular forces [21, 22, 23]. In particular after the results reported in Ref.[22], the free Brownian diffusion was expected to be dramatically reduced by the formation of large molecular clusters when the concentration of the solvated molecules exceeds a critical value. These preliminary results have suggested to experimentally look for this hallmark of the activation of electrodynamic interactions. However, a more advanced and thorough investigation of this clustering transition was in order, thus it has been done in the present work (see [28], section II). By resorting to a semi-analytical model, to Molecular Dynamics simulations, and to Monte Carlo computations it is shown that the activation of electrodynamic forces entails the existence of a first-order clustering phase transition. This transition between a "dispersed" phase and a "clustered" phase occurs at a critical value of the concentration of actively oscillating biomolecules out-of-thermal-equilibrium, therefore at a critical value of the average intermolecular distance. An independent and complementary experimental possibility of detecting the activation of intermolecular electrodynamic forces has been suggested in Ref.[12]. In that case, the frequency of the collective oscillation mode of an isolated macromolecule undergoes a shift when placed close to another macromolecule oscillating at the same frequency. This shift is inversely proportional to the cube of the intermolecular distance. Remarkably, this remains true for a large number of molecules in solution (see [28], section III) in which case the frequency shift is found again to be inversely proportional to the cube of the *average* intermolecular distance. If this represents an experimental crosscheck of the diffusion-based approach, challenge comes *a-priori* from the difficulty in implementing THz spectroscopic measurement of proteins in aqueous solutions due to the strong absorption of water in the THz and sub-THz frequency domains. But this difficulty is considerably reduced when measurements are performed under out-of-equilibrium conditions. In fact, this is distinct from standard spectroscopic measure-

ments, where the incident radiation simultaneously excites the atoms or molecules under study and probes their absorption spectrum by sweeping a range of frequencies. With THz spectroscopy of out-of-equilibrium biomolecules in solution, the analysis is carried out on already active objects (whose vibrations are induced by an internal cascade or interconversion of light), and weak THz radiation is only used to read and detect active vibrations of the biomolecules. Moreover, the absorption of THz radiation by the actively oscillating molecules is much stronger than the absorption of THz radiation by water, thus making molecular absorption features well detectable despite the presence of water.

Two experiments operating in different conditions

In the FCCS setup, the laser beam is focused in a small volume of about one femtoliter where a high energy density is attained. This is necessary to excite the collective oscillation of the R-PE molecules during their quick transit through the confocal volume of transversal diameter of 916 nm. The R-PE molecules efficiently harvest light by means of their 38 fluorochromes within each protein molecule. On the contrary, in the THz spectroscopy setup, a much lower energy density was attained because the laser beam illuminated a large drop of solution of 35 μL. This notwithstanding, the excitation of collective oscillations of both the BSA molecules and of the R-PE molecules, respectively, was attained - without making them cluster - by means of long exposure times. The activation of collective oscillations of the molecules in solution preventing at the same time their clustering (which simply means that the electrodynamic forces were unable to overcome the thermal forces) was a necessary condition, in fact, a clustered fraction of the molecules would have completely altered the relationship between frequency shift and concentration. This operating condition was obtained by adjusting the laser power so as to lower the threshold value of the average intermolecular distance of the clustering transition below 500 $\mathring{A}$ for the R-PE. Moreover, the same laser power density was unable to induce the clustering phase transition of the BSA molecules because the power density was not enough to excite sufficiently strong collective oscillations. This is the reason why the BSA turned out not apt for the experiments based on self-diffusion. In fact, the BSA is not naturally sensitive to light, and, to get excited, its collective oscillation mode requires a very long time of light-pumping via the artificially attached fluorochromes [19]. Long illumination times were realised in the THz setup but this was not possible in the FCS/FCCS setups where the transit times throughout the confocal volume was exceedingly short to activate the collective oscillations of the BSA molecules in spite of the high light power density in the confocal volume. In conclusion,

let us remark that the electrodynamic forces can be active also in the disperse phase when the proteins undergo Brownian diffusion. In other words, even if these forces are not strong enough to make the clustering transition by winning against thermal disorder, they can nevertheless induce the frequency shifts reported in Figure 4.

Biochemical samples

R-PE was purchased from Merck (52412). BSA conjugated to Alexa Fluor^{TM} 488 was purchased from Thermo Fischer Scientific (A13100). Samples were prepared by sequential dilutions of proteins in 200 mM NaCl. Their final concentrations were controlled by absorbance measurements (Nanodrop One Spectrophotometer, Thermo Fischer Scientific) at 566 nm for R-PE (ε = 1 960 000 $M^{-1}cm^{-1}$) and at 280 nm for BSA (ε = 43824 $M^{-1}cm^{-1}$) with a correction factor of 0.11 to account for AF488 at 280 nm.

Fluorescence Fluctuations Spectroscopy experiments

Setup. All fluorescence fluctuation spectroscopy measurements were performed on a confocal microscope (ALBA FCSTM, from ISS Inc., Champaign, USA) with a picosecond/CW 488 nm diode laser (BDL-488-SMN, Becker and Hickl, Germany) used at 80 MHz and focused through a water immersion objective (CFI Apo Lambda S 40X/1.25 WI, Nikon). The fluorescence collected by the same objective is split into two paths by a 50/50 beam splitter (Chroma 21000) and filtered by 525/40 nm band pass (Semrock FF02-525/40) before been detected by avalanche photodiodes (SPCM AQRH series, Perkin Elmer/Excelitas). Signals are recorded by a multitau hardware correlator (FLEX-02-12D, Correlator.com, Bridgewater, NJ).

Data acquisition. Before each experiment, the laser power is adjusted at the back-aperture objective and, the lateral waist value ω calculated knowing the diffusion coefficient of AF488 [$D_{AF488}(20°C)$ = 409 $\mu m^2/s$ derived from [42]] in aqueous solution at 20^o C and according to the equation $\omega^2 = 4D\ \tau_D$. FFS measurements were performed on sample in 8-well LAB-TEK chambers (Thermo Scientific Nunc) at given concentration of proteins diluted in 200 mM NaCl. Five independent experiments were conducted for each condition (protein concentration and laser power) with each individual measure corresponding to a series of 10 measurements lasting 60 seconds. Different strategies have been previously applied to perform FCS measurements at micromolar concentrations [43, 44]. Here, to overcome this concentration limitation, which is mainly due to the detector limits, the collected signal was attenuated by optical density (OD) filters on the path just after the emission filters. The addition of OD1 or OD1.3 filters

with transmission values of 10% and 5%, respectively, allows keeping records with satisfactory amplitude fluctuations and count rates per molecule for reliable analyses. The effectiveness of this experimental approach has been validated with high concentrations of aqueous solutions of the Atto488 dye (Extended Data Figures 7 and 8). In addition, the use of the FCCS data acquisition modality avoids post-pulse artifacts due to spurious photon detection [45].

Data analysis. As mentioned above, all data were collected in a FCCS mode for proper experimental analyses. Consequently, we analyze the fluctuations by a cross-correlation function (CCF) defined as

$$G(\tau) = \frac{\langle \delta F_1(t) \delta F_2(t+\tau) \rangle}{\langle F_1 \rangle \langle F_2 \rangle}\,, \tag{3}$$

with $\delta F_1(t)$ and $\delta F_2(t)$ the signal collected by detector 1 and 2, respectively. The averages are performed over time. We kept simplest the mathematical model fitting the CCF by using the standard analytic form of the function $G(\tau)$ for a one-component system in a 3D environment which reads as [46]

$$G(\tau) = \frac{1}{N}\left(\frac{1}{(1+\tau/\tau_D)\sqrt{1+s^2\tau/\tau_D}}\right), \tag{4}$$

where N is the average number of molecules, τ_D the average diffusion time of the tracer through the confocal volume, and s the structure parameter of the confocal volume, that is, its axial to lateral waist ratio ω_{xy}/ω_z. Still, the fitting accuracy of CCFs with Eq.(4) is no longer very good with high laser power and at high concentrations (Extended Data Figure 12) because of CCF distortion due to very long transit times of protein clusters. Therefore, the CCFs that are no longer accurately fitted by the standard function $G(\tau)$ are preliminarily smoothed by applying a Savitzky-Golay filter using a polynomial of third degree (red curves on Extended Data Figure 12). This allows to get reasonable estimates of τ_D as the lag time corresponding to the half-height of the smoothed CCF. Note that when the R-PE concentration exceeds even slightly a clustering critical value, these estimates are fully acceptable and adequate for our purposes. In fact, in this case τ_D suddenly increases of several orders of magnitude with respect to its Brownian value, thus making the details of its estimation irrelevant. The variation of τ_D is also so large that the effects of the high level of noise at short lag-times on its estimate do not have any meaningful consequence on the clear evidence of the clustering phase transition.

Confocal video-microscopy

The confocal video-microscopy images were performed on a confocal microscope (ALBA FC-STM, from ISS Inc., Champaign, USA) with a picosecond/CW 488 nm diode laser (BDL-488-SMN, Becker and Hickl, Germany) used at 80 MHz and focused through a water immersion objective (CFI Apo Lambda S 40X/1.25 WI, Nikon). The fluorescence collected by the same objective is filtered by a 525/40 nm band pass (Semrock FF02-525/40) before being detected by avalanche photodiodes (SPCM AQRH series, Perkin Elmer/Excelitas). Each 128×128 pixel confocal image is recorded by scanning the field of view with at a pixel dwell time of 0.1 ms.

THz spectroscopy experiments

Long-range interactions between macromolecules can be highlighted through the dependence of their collective oscillation frequency, lying within the THz domain, on intermolecular distance or concentration. THz near-field spectroscopy allows to measure the occurrence of such collective oscillations if one is able to realize this spectroscopy on proteins immersed in saline solution: a well-known technological roadblock, due to the huge absorption of THz radiations by water. We thus have developed two specific setups to overcome this limitation operating in the 0.07-0.11 THz domain and in the 0.25-0.37 THz range, respectively.

1. Rectenna-based THz-spectroscopy.

Setup. For the 0.07 to 0.11 THz band, a continuous-wave (CW) THz radiation was generated by a Virginia Diodes WR10 source with 25 mW output power. A droplet of 30 - 35 μL of a solution of R-PE (see Methods) was filed into a 14-pin ceramic dual in-line package (DIL) forming a cuvette where the rectenna (a bow-tie antenna connected to a GaAs/AlGaAs high-electron-mobility transistor) is placed (Figure 5(a)). A plastic-(transparent to blue and THz radiations) film was used to seal the system and to reduce evaporation. To excite the proteins, a Spectra Physics^{TM} blue laser (ExcelsiorOne 488C-50) emitting at 488 nm and delivering a maximum of 50 mW output-power was focused onto the detector. The laser output-power is controlled by a set of optical-density filters.

Data acquisition. THz passing through the solution of water, NaCl and excited protein is detected by the rectenna providing a DC-voltage at its loads, proportional to the THz-field intensity. While the dimensions of the rectenna reach half-a-wavelength (at 0.3 THz), the THz-field is only enhanced in the feed-gap region of the antenna e.g. within a volume of about 0.2 pL. A hydrophobic, biocompatible and transparent to both THz and blue radiations varnish was applied to the upper layer of the rectenna. Experiments were done at room temperature.

Data analysis. Normalization procedure, according to Beer–Lambert law, divides spectra of proteins in solution under illumination $I_{R-PE_{ON}}$ by spectra of proteins in solution without illumination $I_{R-PE_{OFF}}$. To obtain spectra of excited proteins only – A is thus proportional to the absorbance coefficient of excited proteins – the result is then divided by the buffer spectra I_{NaCl} (also with and without illumination).

$$A = \log\left(\frac{I_{R-PE_{ON}} \div I_{R-PE_{OFF}}}{I_{NaCl_{ON}} \div I_{NaCl_{OFF}}}\right) .$$

Savitsky – Golay smoothing was used at the end to smooth curves, with 15 points of window and a polynomial order of 2.

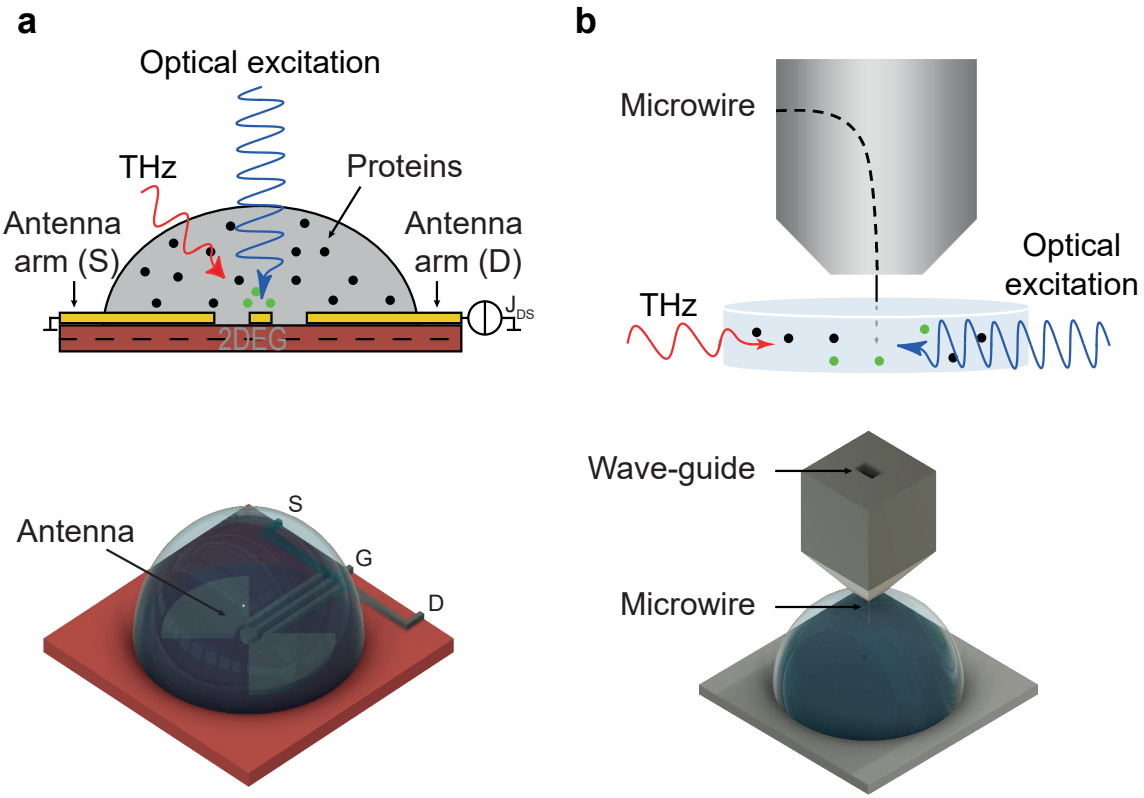


Figure 5: THz-spectroscopy experimental setups. (a) Rectenna for the 0.07 to 0.11 THz band; (b) Microwire-based probe for the 0.25 to 0.37 THz band.

2. Microwire-based probe.

Setup. For the 0.25 to 0.37 THz band, CW-THz radiation is produced by a Signal Generator Extension (SGX) module designed by Virginia Diodes, Inc. Module WR9.0 (82-125 GHz) SGX was used with external multiplier WR2.8 to extend the frequency coverage to 0.25-0.37 THz with an average power of 1 mW. The radiation emitted is then collimated and focused by PTFE lenses on the biological sample. Optical excitation, represented by a blue laser and a UV lamp, was used to excite different components of the protein under study. Thus, for the

optical excitation of fluorochromes, a Cobolt 06-MLD laser was used emitting an output-power of 40 mW at the wavelength of 488 nm. Optical excitation of aromatic amino acids included in the protein was performed using LED M275L4 produced by ThorLabs at a wavelength of 275 nm and a typical output-power of 60 mW. Due to its large numerical aperture (NA=0.86) UV-coated lenses were used to collimate and focus the radiation onto the sample. Thus, a spot size of about 1cm in diameter was achieved. A micro-coaxial near-field wire (Figure 5(b)) is inserted inside a metallic rectangular waveguide to allow a modal transition from TM01 Sommerfeld's mode to TE01 waveguide mode. The probe is capable of highly localized detection of the longitudinal component of the electric field [47] due to the sub-wave diameter of the wire around 10 μm at the tip into the volume of about 4 pL.

Data acquisition. A specific sample holder was also designed. It is constituted by a plastic cylinder, transparent to UV, blue and THz radiations and resistant to UV radiation with a diameter of 7 mm and a volume of 53 μL. At its bottom, a 130 μm-thick glass was used, through which laser excitation was performed. To avoid evaporation and, as a consequence, changes in protein concentration during the experiment, the sample was covered by a plastic film with a thickness of 5 μm, allowing the wire to pass through it without damage.

Data analysis. Regarding the normalization, the same procedure than in rectenna experiments has been followed, according to Beer–Lambert law, to obtain spectra of excited proteins only. However, since in this frequency-band (0.25 - 0.37 THz) the signal-to-noise ratio is poor due to high absorption by water molecules, a specific data processing and normalization procedure (using a band-stop Fourier transform filtering and Lorentz functions fitting) has been followed to extract an usable signal and frequencies of collective-oscillation resonances.

It is thus possible to observe the evolution of the absorption-peak amplitude as a function of the duration of illumination. Were considered as absorption peaks, those whose height and area are increasing continuously with time. Time (up to 1 hour) and concentration (from 750 to 60,000 nM) dependences of the THz-spectra have been characterized.

Data Availability

The data that support the findings of this study are available from the corresponding authors upon request. Theoretical models to interpret the experimental outcomes, as well as videos showing the formation of clusters, are available in the online version of the paper.

Code Availability

The codes that are used in this study are available from the corresponding authors upon request.

Acknowledgements

The project leading to this publication has received funding from the Excellence Initiative of Aix-Marseille University - A*MIDEX, a French "Investissements d'Avenir" programme. This work was also partially supported by the Seventh Framework Programme for Research of the European Commission under FET-Proactive grant TOPDRIM (FP7-ICT-318121), by the projects SIDERANT and NEBULA financed by the french CNRS, by the Occitanie Region and by Montpellier University through its TOP platform and by the LabEx NUMEV (ANR-10-LABX-0020) within the I-Site MUSE. We acknowledge the PICSL imaging facility of the CIML (ImagImm), member of the national infrastructure France-BioImaging supported by the French National Research Agency (ANR-10-INBS-04).This project has also received funding from the European Union Horizon 2020 Research and Innovation Programme under the Marie Skłodowska-Curie grant agreement No 765426 (TeraApps). The authors would specifically thank the European Commission through the European Innovation Council (EIC) Task Force which, on the basis of the results presented in this article, has awarded the FET-Open LINkS project, grant No 964203.

Authors Contributions

M.L., Y.M., M.G. have been crucial for the success of the project. M.L. designed and performed all the experiments in Marseille regarding diffusion, he fixed the problem of operating the FCCS at high concentrations, and made the successful choice of the proteins to be studied. M.G. performed all the theoretical modelling and the related Molecular Dynamics and Monte Carlo numerical computations. Y.M., S.R. and A.K. carried out the experiments in Montpellier concerning THz-spectroscopy using the rectenna sensor and the micro-wire probe, both used for intramolecular collective vibration and frequency shift measurements. I.N. participated in the project from its very beginning many years ago paving the way to the present findings and suggested that ED forces could be detected through the frequency shift reported here. E.F. participated in the project from its very beginning and contributed the theoretical part of the paper. S.M. and D.M. gave fundamental support to perform the FCS and FCCS experiments. P.F., F.T. and L.V. participated in the project supporting it since its very beginning many

years ago. J.S. contributed on the biophysical and biochemical aspects of the work. J.T., with the support of D.C. and S.R., conceived, designed and built the experimental setup in Montpellier and supervised the experiments. M.P., in quality of project leader, initiated this research many years ago and designed, supervised and intervened in all the theoretical and experimental aspects of the project. All the authors contributed to the discussion and to the analysis of the results. M.P. wrote the paper with the help of J.T., D.M., J.S., M.G., M.L., S.R., E.F., L.V..

Corresponding author

Correspondence and requests for materials should be addressed to M.P. and J.T.

Competing interests

The authors declare no competing financial interests.

Additional Information

Extended Data

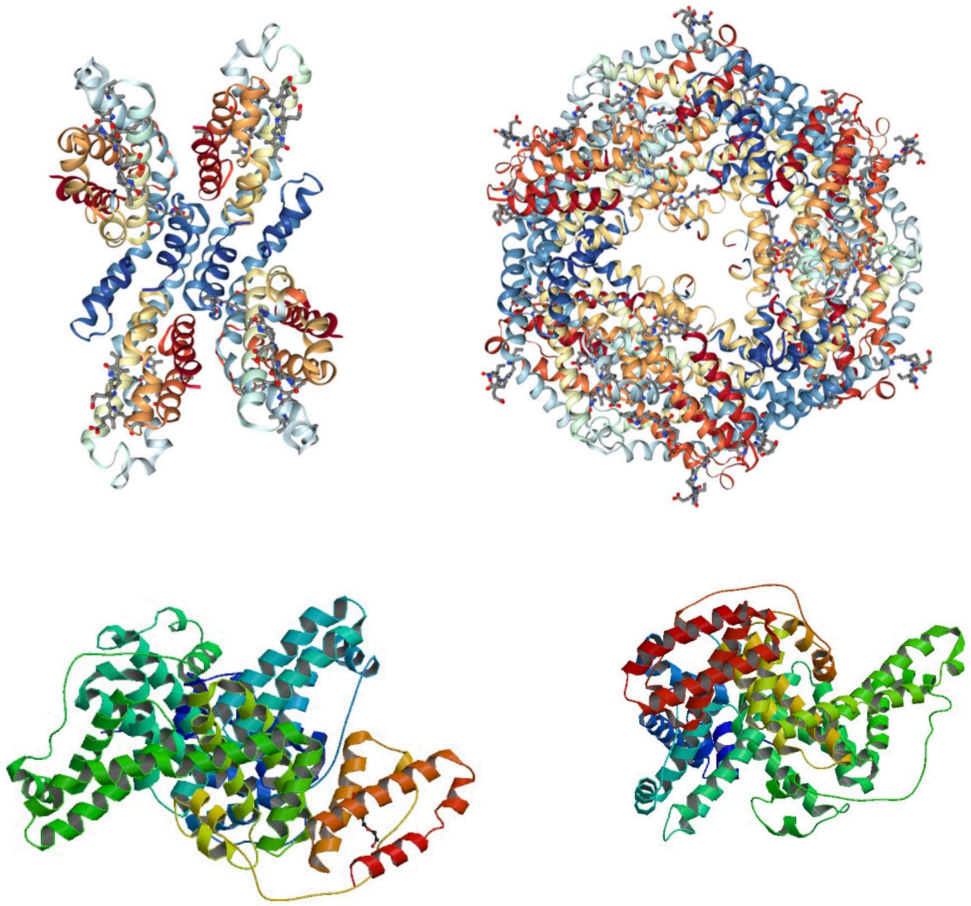


Figure 6: Images from Protein Data Bank. Top right, the assembly $\alpha_2\beta_2$ which forms a subunit (1EYX) of the R-PE protein. Top left, a unit of R-PE $(\alpha_2\beta_2)_3$. Bottom images: Two different projections of the BSA (3V03). It is clearly seen that both proteins are mainly made out of alpha-helices.

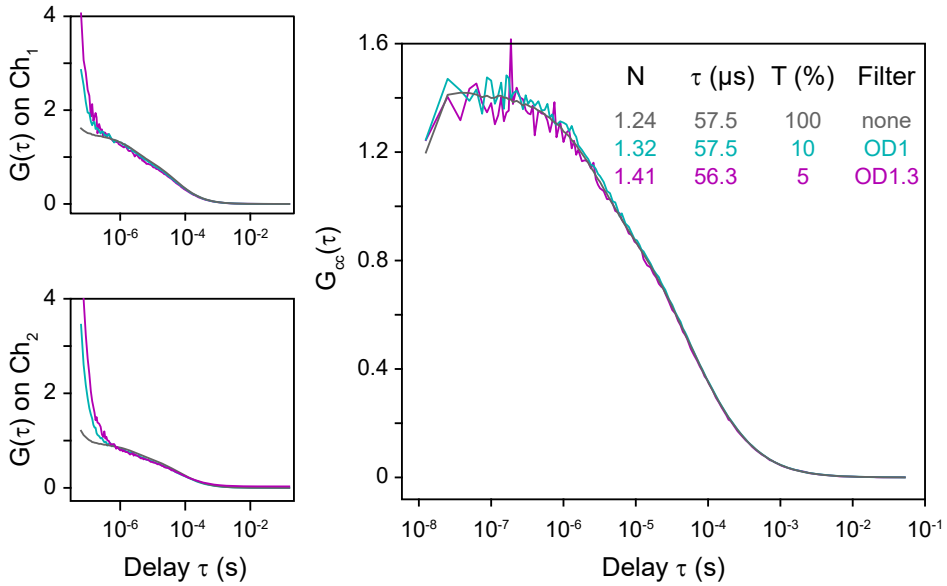


Figure 7: CCFs in the presence of micro-molar concentrations of fluorescent dyes obtained with density filters along the optical path combined with averaging during long acquisition times. The left panel shows the comparison of Cross-Correlation Functions (CCFs) of a single solution of the dye Atto 488 at the concentration of 1 nM, measured without OD (Optical Density) filter (no OD, black line) along the fluorescence path, with OD1 and with OD1.3 (cyan and magenta lines, respectively). Panels on the right show the Auto-Correlation Functions (ACFs) obtained with the signals of channels 1 and 2 for the same measurements. At short time-lag the ACFs clearly show a sharp increase, whereas this phenomenon is absent on CCFs. The phenomenon is consequently an artifact attributed to afterpulsing. Each CCF was obtained by averaging 72 CCFs, each one obtained from a record of 50 seconds, corresponding to an overall acquisition time of one hour.

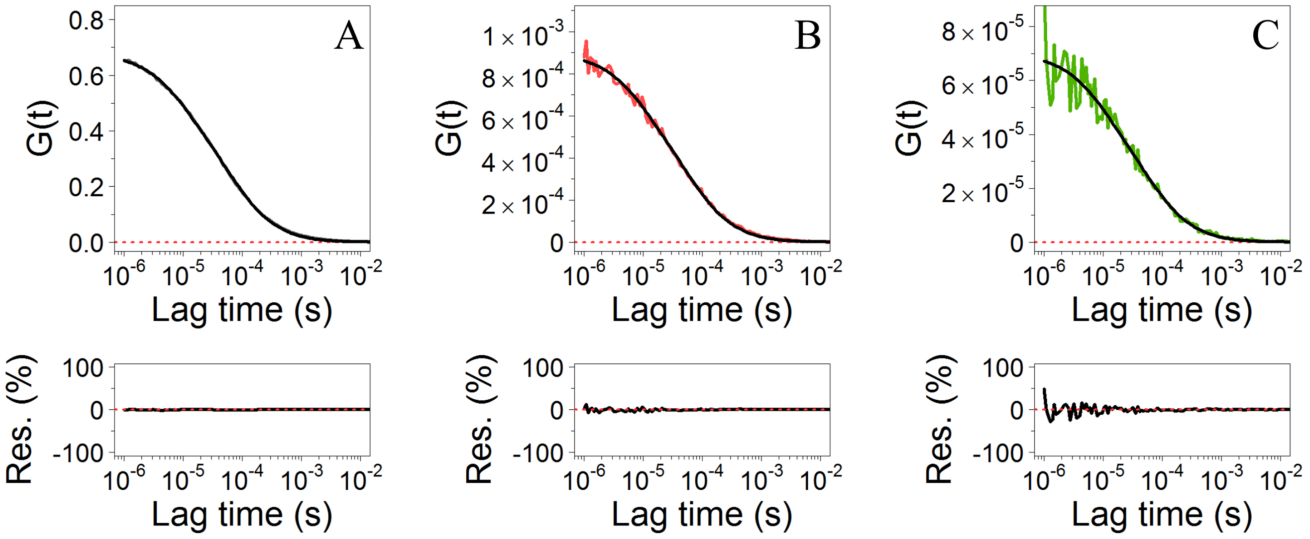


Figure 8: FCCS results at high concentrations of fluorescent molecules and using density filters. Panels A to C display the CCFs - as shown in Figure 7 - corresponding to solutions of 1 nM, 1 μM, and 10 μM of Atto 488 dye using no OD filter, OD1, and OD1.3 filters, respectively. Each CCF was obtained by averaging 72 CCFs, each one obtained from a record of 50 seconds, corresponding to an overall acquisition time of one hour. The fitting curves are also displayed in black on each panel, and the residuals are visible below each CCF (displayed in percentage). The same values of τ reported in Figure 7 are found within a 2% deviation.

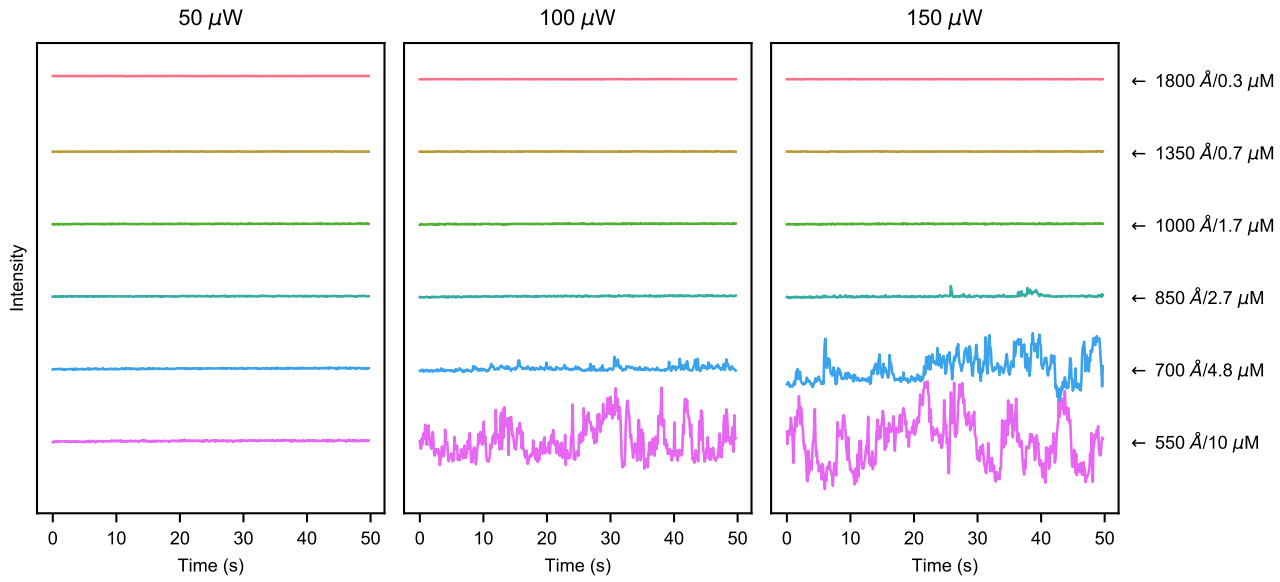


Figure 9: Traces recorded by channel 1 of the FCCS device during 60 seconds, for solutions of R-PE. The average distances among the proteins are, from top to bottom, respectively: 1800 Å, 1350 Å, 1000 Å, 850 Å, 700 Å, 550 Å. The left panel shows the results for the laser output power set at 50 μW, middle panel for the laser power set at 100μW, and right panel for the laser power set at 150 μW. The sharp increase of fluorescence fluctuations at increasing laser power and protein concentration is due to the formation of clusters as shown by the on-line Videos.

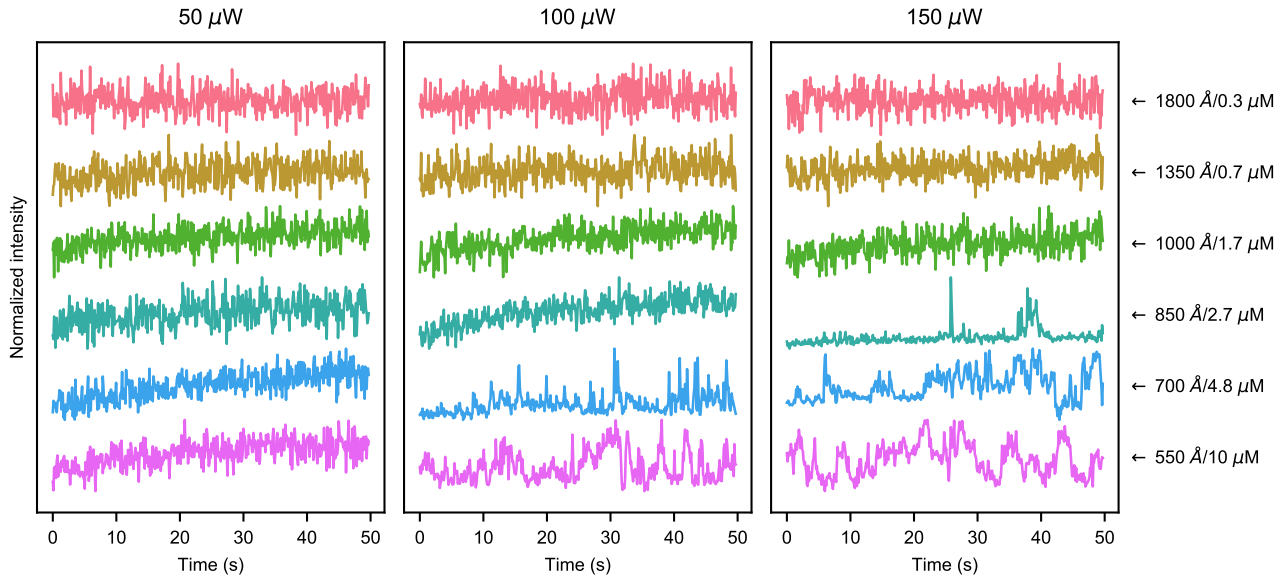


Figure 10: The same outcomes of Extended Data Figure 9 are here shown by normalizing the data to the highest fluorescence value recorded for each trace. Fluorescence traces recorded by channel 1 of the FCCS device during 60 seconds, for solutions of R-PE. The traces are normalized by the highest value of each trace.

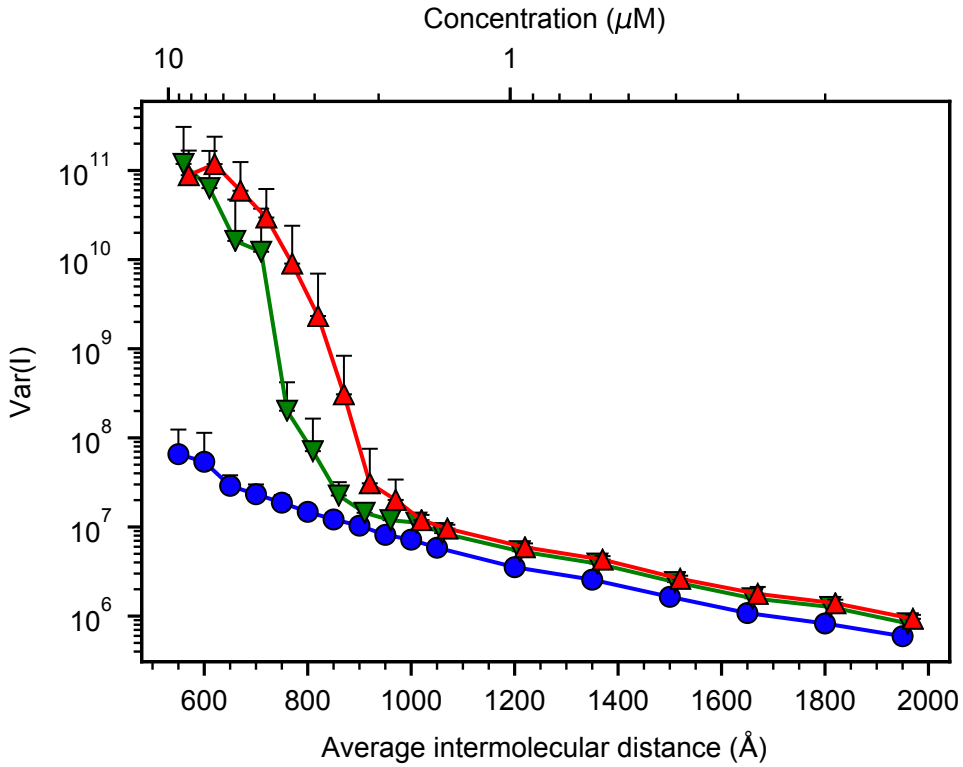


Figure 11: Variance of the fluorescence intensity recorded for R-PE solutions at different laser power input: 50 μW (blue circles), 100 μW (green down-pointing triangles), and 150 μW (red up-pointing triangles). Only upper error bars are shown on this plot for convenience, as the y axis is on a logarithmic scale.

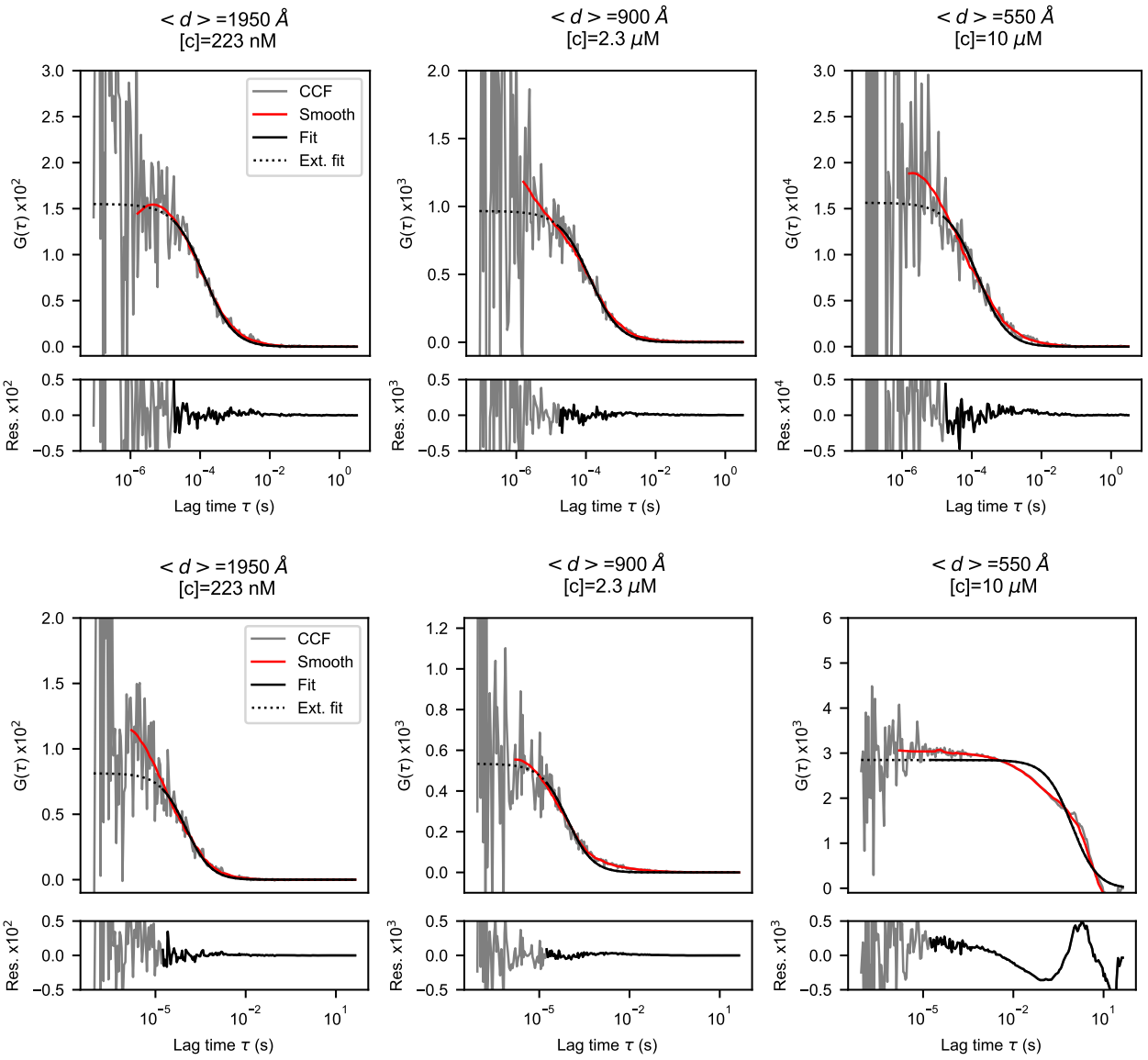


Figure 12: Cross-Correlation Functions (CCFs) for R-PE solutions at different concentrations. From left to right the average intermolecular distances are: $\langle d \rangle = 1950$ $\mathring{A}$, $\langle d \rangle = 900$ $\mathring{A}$, $\langle d \rangle = 550$ $\mathring{A}$, respectively. The upper panels display the results obtained with a laser power input of 50 μW (grey lines). The lower panels display the results obtained with a laser power input of 150 μW (grey lines). A Savitzky-Golay filter is used to smooth the CCFs (red lines), and to consequently obtain the diffusion time τ_D at Half Height (THH). Fits of the CCF are also shown (black lines), and the extended fits (outside of the original fitting range) are represented with dashed lines. Residuals of the fits are also plotted: the black lines correspond to the standard residuals, and the grey lines to the extended residuals. At the highest concentration, for $\langle d \rangle = 550\mathring{A}$, and laser power input of 150 μW, the correlation time is increased by several orders of magnitude, entailing a drop of the diffusion coefficient by the same amount.

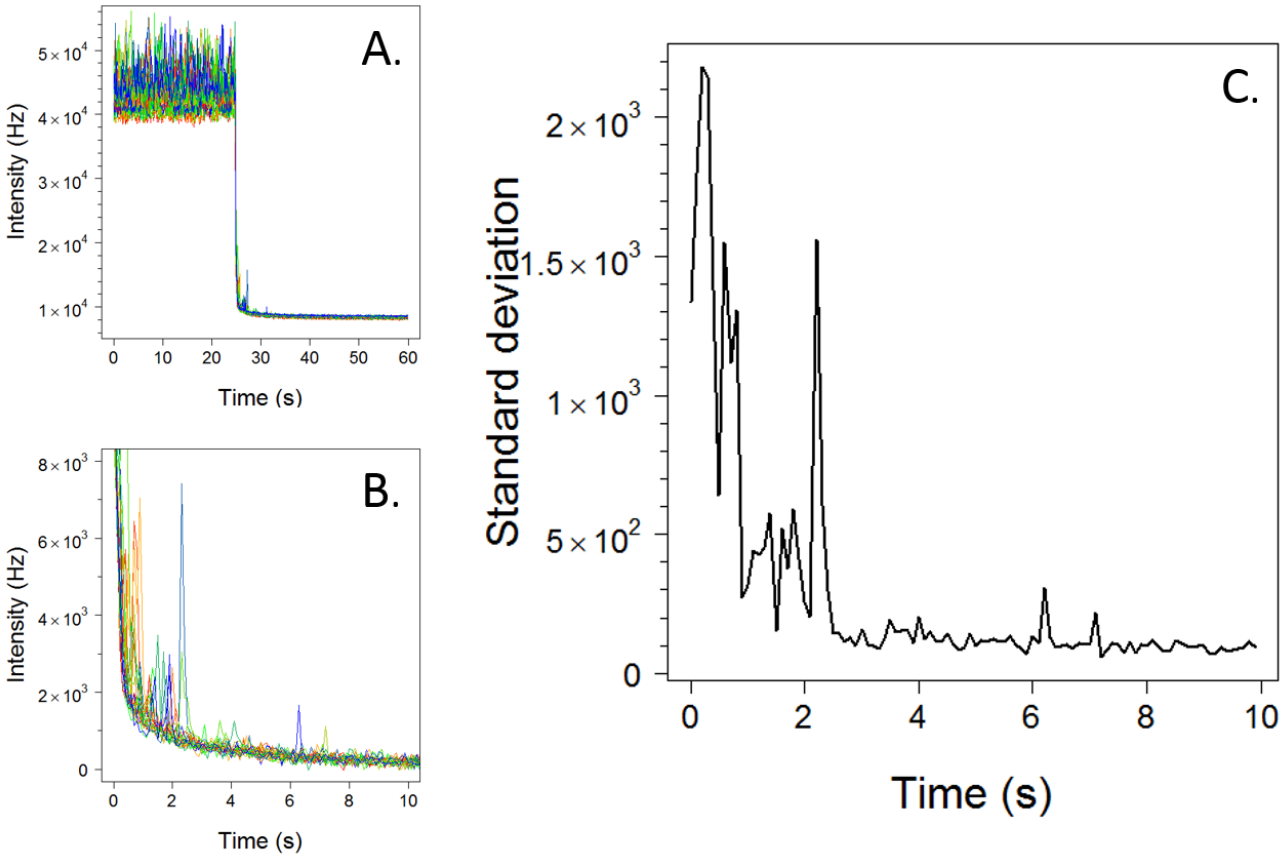


Figure 13: Decay of the clusters of R-PE induced by a sudden lowering of the laser power density. The results reported here have been obtained using ten samples corresponding to an average intermolecular distance of 650 $\AA$. On panel A, the laser input has been lowered from 150 μW to 50 μW at $t = 25$ s. Panel B is a zoom of panel A, starting at $t = 25$ s. Panel C is the standard deviation of the intensity of the different samples recorded and displayed by panels A and B. Here the thermal fluctuations overcome the attractive electrodynamic forces weakened by the lowering of the energy input rate, thus destroying the clusters. The initial time $t = 0$ has been arbitrarily chosen in the already clustered phase.

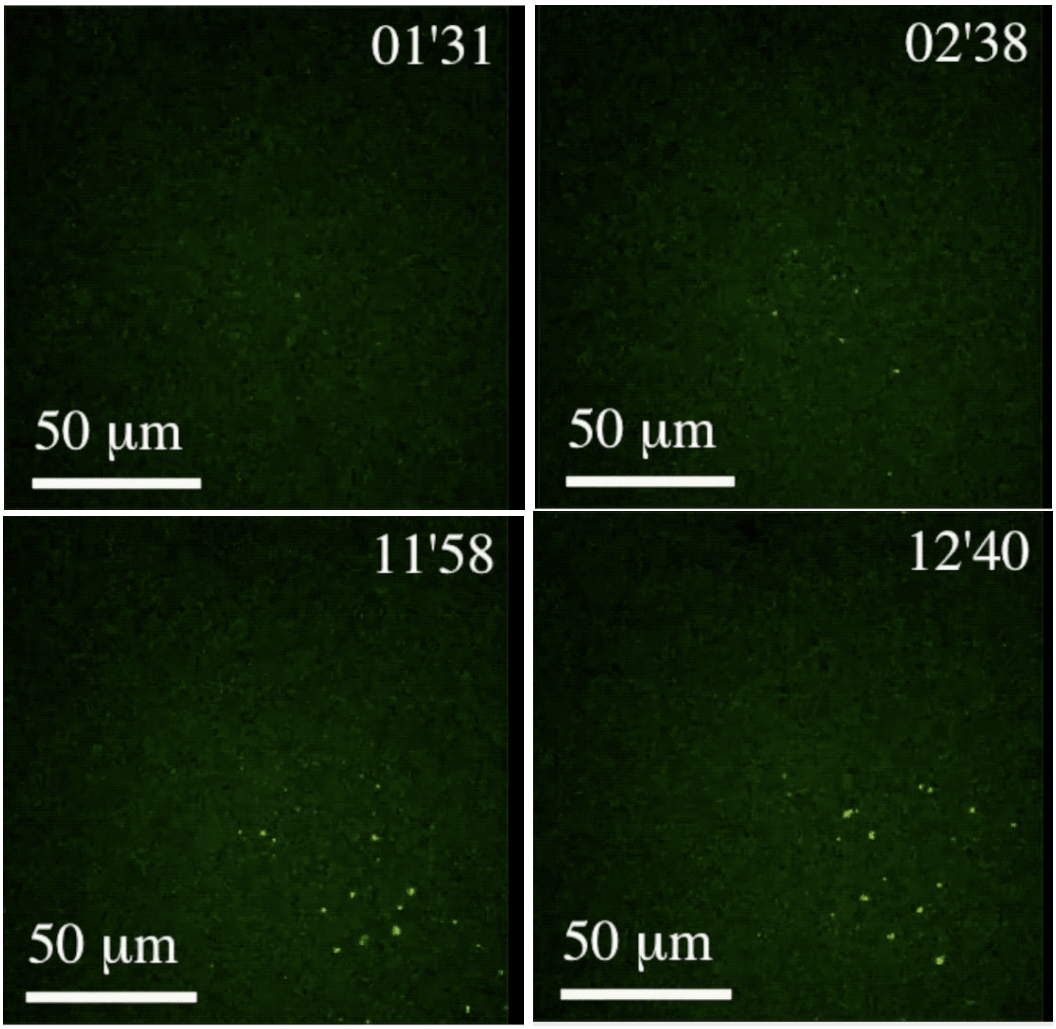


Figure 14: Screenshots saved out of a video of a solution of R-PE with an average molecular distance of 800 $\mathring{A}$ and laser power of 150 μW (the video is available online). The snapshots have been saved at times t=1min 31s (higher left panel), t=2min 38s (higher right panel), t=11min 58s (lower left panel) and t=12min 40s (lower right panel). The formation of protein clusters is well evident.